Editors' Suggestion

Edge-Plasmon Whispering-Gallery Modes in Nanoholes

M. Lorente-Crespo,[1] G.C. Ballesteros,[2] C. Mateo-Segura,[1] and C. García-Meca[3,*]

[1] *Institute of Sensors, Signals and Systems, Heriot-Watt University, Edinburgh EH14 4AS, United Kingdom*
[2] *Institute of Photonics and Quantum Sciences (IPaQS), Heriot-Watt University, Edinburgh EH14 4AS, United Kingdom*
[3] *Nanophotonics Technology Center, Universitat Politècnica de València, Valencia 46022, Spain*

(Received 25 June 2019; revised manuscript received 23 November 2019; accepted 24 January 2020; published 20 February 2020)

Metallic apertures remain one of the most intensively investigated optical structures due to their rich behavior. This encompasses physical phenomena such as Bragg scattering, surface plasmons, or localized modes, offering great potential for many applications in the growing fields of nanophotonics and plasmonics. Here, we show that isolated metallic nanoholes can additionally support edge plasmons in the form of whispering-gallery modes and we demonstrate that, although high-order modes remain dark at normal incidence, they can be excited at oblique illumination. As revealed by simulations, the existence of these modes in nanohole arrays is fundamental to understanding complex resonant phenomena and to explaining previous unexpected experimental results found in metamaterials. Notably, the symmetries of the employed lattice determine the excited mode orders, which, together with a strong dependence on the film thickness, yields an easily and highly tailorable optical response. Furthermore, some modes display unusually narrow line widths (approximately 7 nm) and a high sensitivity to the environment, resulting in one of the highest sensing figures of merit (approximately 80) reported for a localized plasmon. These singular features may find application in the construction of special polarizers and filters, single-layer zero-transmittance absorbers, and high-performance nanosensors.

DOI: 10.1103/PhysRevApplied.13.024050

I. INTRODUCTION

A whispering-gallery mode (WGM) is a kind of wave that loops around the surface of a cavity (typically with a circular or spherical shape) due to continuous total internal reflection. Optical WGMs have been widely used across the whole electromagnetic spectrum [1–3] and have an ample range of applications, from on-chip photonic filters and biosensors to ultralow-threshold lasers [4]. Surface plasmon polaritons (SPPs) are a special type of electromagnetic wave confined to the surface of conductors and, as such, can also appear in the form of WGMs [5,6].

On the other hand, it is well known that finite metal films not only support SPPs propagating along two-dimensional (2D) interfaces, but also edge modes with reduced dimensionality, i.e., one-dimensional edge plasmons (EPs), which are highly confined to the ridges of the film [7]. Recently, it has been shown that this kind of SPP remains mostly unaltered when curvature is introduced, even for bending radii as small as a few tens of nanometers [8]. As a result, the ridge modes appearing in straight films can become EP-WGMs if a disk is formed by bending the film [Figs. 1(a) and 1(b)]. In that work, *Schmidt et al.* experimentally demonstrated the existence of these modes and showed that a standing wave exhibiting a specific number of field antinodes—a WGM—appears if the condition for constructive interference is met. However, it has so far been overlooked that film bending may also lead to a completely different scenario: the creation of a nanohole [Fig. 1(c)].

This suggests that nanodisks and nanoholes can be understood as particular cases of convex and concave bends, respectively. In general, these two kinds of structures have experimentally proved to exhibit a similar optical behavior for both isolated particles and disordered arrays [9,10]. Therefore, the existence of EP-WGMs circling along the ridges of nanoholes should be naturally expected. This is supported by the observation of an edge mode with dipolar character in an isolated nanohole by *Degiron et al.* [11] and later related studies [10,12]. Notably, nanohole EP-WGMs resemble the original acoustic WGMs discovered by Lord Rayleigh [13] more closely than nanodisk EP-WGMs.

This work is thus aimed at showing that the dipolar modes reported in Ref. [11] and similar works are just the lower-order EP-WGMs of the nanohole. Moreover, we prove that higher-order multipolar modes become accessible to free-space light at oblique incidence. Our

*cargarm2@ntc.upv.es

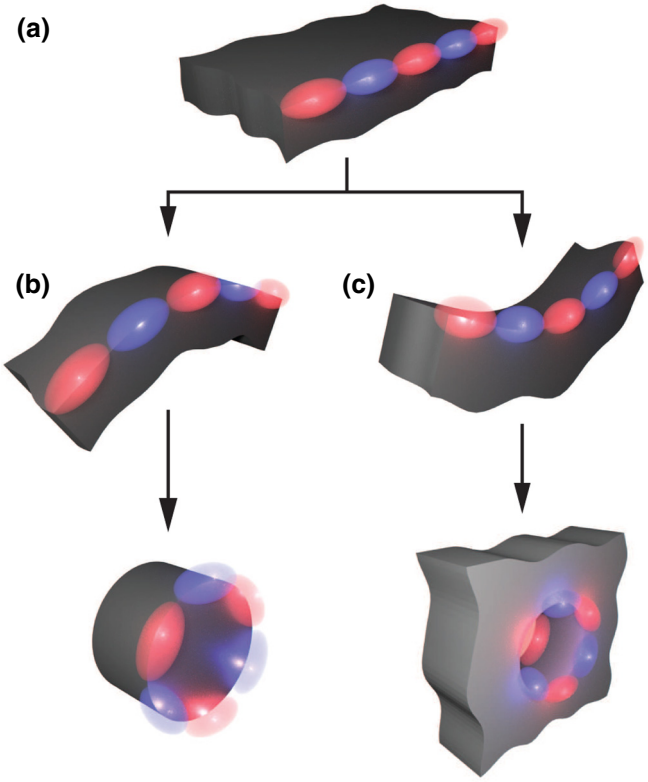

FIG. 1. The transformation from straight to curved edges: from (a) a straight metallic edge to (b) a nanodisk following a convex bend and (c) a nanohole following a concave bend.

findings serve to explain previous unexpected experimental results found in negative-index metamaterials [14] as well as other complex resonant phenomena involving various combined mechanisms [15–17]. Additionally, the studied EP-WGMs exhibit several remarkable features of interest for applications such as biosensing, optical filtering, and the realization of special polarizers and absorbers.

II. RESULTS

The modes supported by circular nanoholes with radius r drilled into a free-standing silver film with thickness t are the focus of this study. The optical response of isolated nanoholes is initially investigated via finite-difference time-domain simulations using LUMERICAL [18]. In this case, a total-field scattered-field source is assumed as the excitation. Such a source emits plane waves while enabling the automatic separation of the scattered field from the total field. In addition, EP-WGMs in nanohole arrays are analyzed through full-wave simulations performed with CST MICROWAVE STUDIO. In the following and without loss of generality, the film is considered to be parallel to the x-y plane, as shown in Fig. 2(a). The permittivity of silver is described using a Drude model with a plasma frequency $\omega_p = 1.37 \times 10^{16}$ rad/s and a damping constant $\Gamma = 40$ THz [19].

A. Isolated nanoholes

To demonstrate the existence of the aforementioned EP-WGMs, it is instructive to analyze the optical response of isolated nanoholes. As a representative example, a film with $t = 30$ nm and a hole with $r = 160$ nm is initially studied (Fig. 2). The scattering cross section σ_{scat} normalized to the area D of the nanohole when illuminated by a p-polarized plane wave is depicted in Fig. 2(b). At normal incidence ($\theta = 0°$), a single maximum arises in the scattering spectrum, at a frequency $f \approx 340$ THz. Figure 2(d) illustrates the absolute value of the corresponding

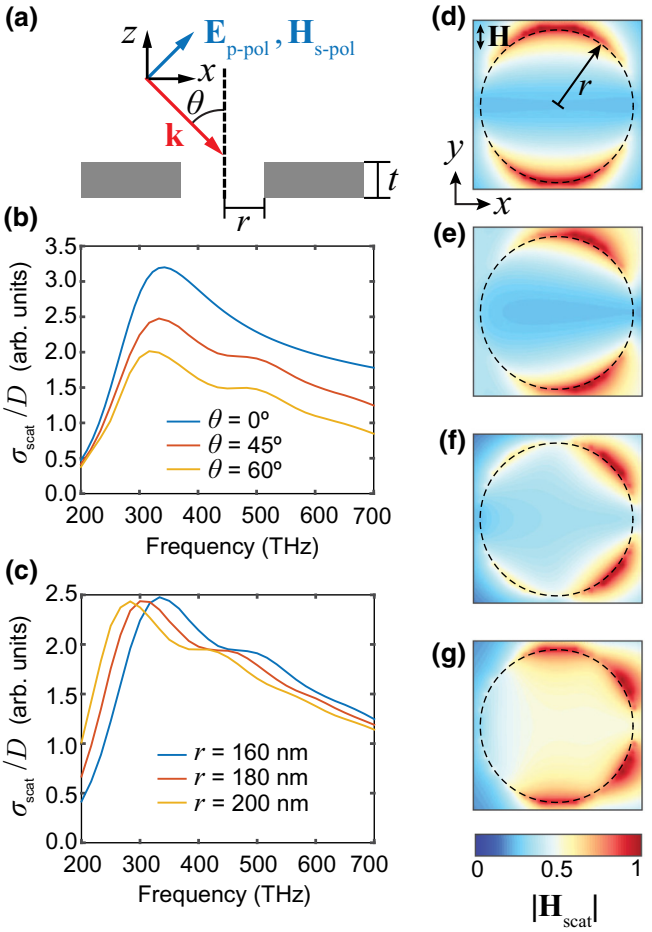

FIG. 2. The optical response of isolated nanoholes. (a) The structure under consideration and the field polarization. The blue arrow represents the **E** field for p polarization and the **H** field for s polarization. (b),(c) The normalized scattering cross section for the $t = 30$ nm case when (b) $r = 160$ nm and θ varies between 0° and 60° and (c) $\theta = 45°$ and r varies between 160 and 200 nm. (d)–(g) $\mathbf{H}_{\text{scat}}$ at the input interface at a frequency of (d) 340 THz, (e) 333 THz, (f) 510 THz, and (g) 660 THz. The angle of incidence is as follows: (d) $\theta = 0°$; (e)–(g) $\theta = 45°$.

scattered magnetic field distribution $\mathbf{H}_{\text{scat}}$ at the film input interface, with $\mathbf{H}_{\text{scat}} = \mathbf{H}_w - \mathbf{H}_{\text{wo}}$, $\mathbf{H}_w$ and $\mathbf{H}_{\text{wo}}$ being the total magnetic field with and without a hole, respectively. Clearly, the field is concentrated at the edges of the hole and exhibits a dipolar character. Remarkably, as the angle of incidence increases, new resonances arise in the spectrum [Fig. 2(b)], which, according to Figs. 2(e)–2(g), correspond to multipolar edge modes. Specifically, the dipolar resonance remains at approximately the same frequency as in the $\theta = 0^\circ$ case [Fig. 2(e)], while a second maximum arises at a higher frequency ($f \approx 510$ THz) as a result of the excitation of a quadrupolar edge mode [Fig. 2(f)]. A hexapolar resonance can also be distinguished at $f = 660$ THz [Fig. 2(g)], although it is much weaker. Along the same line, higher-order modes are expected at higher frequencies. These results allow us to identify the observed resonances as different orders of an EP-WGM. In particular, only the first-order EP-WGM (dipole) is excited at $\theta = 0^\circ$, as this is the unique order possessing the correct symmetry to be excited by a normally incident plane wave, which is dipolar in nature. Nevertheless, higher-order modes, which remain dark at normal incidence, can be excited at oblique illumination due to the symmetry breaking introduced by phase retardation. Indeed, as the angle of incidence increases, the relative contribution of higher-order modes to σ_{scat} is larger. These observations reveal that no additional bright mode is required for their coupling to free-space light, in contrast to other localized modes appearing in similar structures [20]. Note that the observed asymmetry in the field profiles is a mere consequence of the oblique illumination and that the resonant frequencies are almost independent of the angle of incidence, as expected for localized modes. On the other hand, the studied EP-WGM should not be confused with the well-known waveguide or cavity modes that can also appear in nanoholes [17,21–23]. The two modes are different and can coexist at different frequencies. A clear example is provided below in relation to the experimental observation of a quadrupolar EP-WGM. Furthermore, the wavelength λ_m of a given WGM must be a submultiple of the perimeter of the hole (i.e., $\lambda_m = 2\pi r/m$, m being a natural number representing the mode order). To verify this property, a parametric study of the nanohole spectra at $\theta = 45^\circ$ as a function of the value of r is presented in Fig. 2(c). Here, the various scattering peaks red shift for increasing values of r. Note that the higher-order resonances are broader in frequency due to increased losses. However, the condition for constructive interference is still satisfied.

B. Nanohole arrays

Nanoholes are more commonly found in the form of 2D periodic arrangements. Metallic hole arrays offer additional degrees of freedom for tailoring their interaction with light, broadening the range of potential effects and applications [24–26]. Among these, negative-index metamaterials [14,27] and extraordinary-optical-transmission (EOT) structures [28] stand out. The former are the base of the so-called perfect lens and other advanced optical devices [27], while the latter find application in optoelectronics, biosensing, or beaming [29]. Notably, the literature on EOT shows that transmission through hole arrays is a complex phenomenon in which various coupled effects "such as Bragg scattering, SPPs, and localized modes" are involved [17,22,23,29–31]. EP-WGMs may also appear when the nanoholes are arranged in groups; thus, understanding the properties of EP-WGMs in this specific situation is crucial for a better comprehension and an accurate prediction of the optical response associated with this kind of structure. In the following, 2D arrays of nanoholes forming a square lattice with period a are analyzed.

Figures 3(a) and 3(b) show the angular transmittance and absorption spectra for $t = 30$ nm, $r = 160$ nm, $a = 400$ nm, and p-polarized plane-wave incidence. The absorption is calculated as $A = 1 - T - R$, where T and R denote the zeroth-order transmittance and reflectance, respectively. When $\theta \neq 0^\circ$, three different modes, leading to minima (maxima) in the transmission (absorption) spectra, can be distinguished. These are the second-, third-, and fourth-order WGMs (at $f = 460$ THz, $f = 585$ THz, and $f = 660$ THz, respectively). Figures 3(d)–3(f) show the corresponding normalized z component of the magnetic field (H_z) at the hole center for off-normal illumination, which exhibits the different expected multipolar patterns; namely, from lower to higher frequencies, a quadrupole [Fig. 3(d)], a hexapole [Fig. 3(e)], and an octupole [Fig. 3(f)]. These results are in good agreement with those obtained in the case of isolated holes, although slightly red shifted. This shift is attributed to the interaction between adjacent nanoholes via near-field coupling [9,32,33].

In addition, our results show that the EP-WGM resonant frequencies depend very weakly on the angle of incidence, confirming that they are not enabled via grating coupling. An exception to this occurs when WGMs appear interfered by Wood's anomalies (WAs) [34,35] [see the dashed lines in Figs. 3(a)–3(c)]. A WA arises when a grating order changes its character from evanescent to propagating. In this situation, the zeroth-order scattering response may suffer strong variations, such as frequency shifts or increased damping [36]. Note that the magnetic field of the studied EP-WGMs is mainly z directed. Therefore, the excitation via p-polarized waves is basically mediated by the electric field, as in this case H_z is zero. However, s-polarized plane waves have a nonvanishing H_z component, which results in a more complex coupling mechanism, as both the electric and magnetic fields of incident light and EP-WGMs overlap. Actually, as shown in Fig. 3(c), the quadrupole is not excited for this polarization, while the third band does not correspond to a pure octupole as in the case

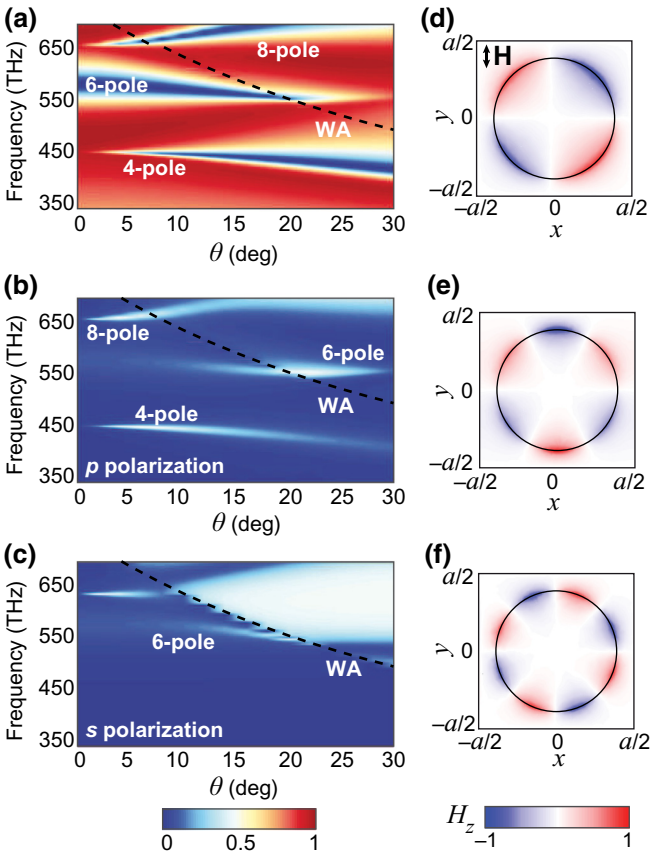

FIG. 3. The optical response of periodic hole arrays. The geometrical dimensions are $t = 30$ nm, $r = 160$ nm, and $a = 400$ nm. (a)–(c) Angular spectra for (a) p-polarization transmittance, (b) p-polarization absorption, and (c) s-polarization absorption. The first-order Wood's anomaly is indicated with dashed lines. (d)–(f) Normalized H_z at the hole center for p polarization, $\theta = 5°$, and (d) $f = 457.5$ THz, (e) $f = 583$ THz, and (f) $f = 661.4$ THz.

of p polarization (the nature of this mode changes with frequency).

C. Tailoring the optical response via lattice symmetries

Figure 3(a) reveals another interesting feature of the studied structure: the third-order EP-WGM (hexapole) is unexpectedly excited at normal incidence. This brings to light the fact that the lattice plays a key role in enabling the coupling of light to some EP-WGMs orders, which would not be excited in isolated nanoholes. This can be explained by considering the symmetries of the structure. In particular, excitation at normal incidence can only occur when the interaction between neighboring holes modifies the EP-WGM in such a way that the symmetries that prohibit its excitation are broken (i.e., if the resulting field distribution has the symmetries of a dipole).

The symmetries that a given mode will exhibit, once it is hosted by the lattice, are given by the intersection of its symmetry group and the point symmetry group of the lattice. For example, the point symmetry group of a square lattice is the dihedral group of order 8 (D_8). The symmetries of an mth-order multipole are D_{2m}, which correspond to a regular even polygon with vertices alternating in color [see Fig. 4(a)]. If the result of intersecting the sets D_8 and D_{2m} is D_2 (i.e., the symmetry group of a dipolar mode), then the mth-order EP-WGM can be excited by a plane wave at normal incidence. This is the case of modes with an odd order $m = 2k + 1$, $k \in \mathbb{N}$ (the symmetry group of which is D_{4k+2}), for which the interaction between horizontal and vertical neighboring holes can be different, and a net dipole moment can be introduced [see the 6-pole case shown in Fig. 4(b)].

However, if the result of the intersection is D_l with $l \geq 4$, excitation at normal incidence is prohibited. This is the case of even-order modes (the symmetry group of which is D_{4k}). Since $D_4 \subset D_{4k}$, i.e., the symmetries of the 4-pole are within the symmetries of the original multipole, and $D_4 \subset D_8$—that is, the symmetries of the 4-pole are a subgroup of the symmetries of the lattice—these modes cannot be excited at normal incidence [see the 4-pole and 8-pole examples in Fig. 4(b)].

A similar reasoning can be followed to show that the first mode to be excited at normal incidence within a hexagonal lattice (with point symmetry group D_{12}) will be a decapole [the third-order mode (6-pole) cannot be excited because $D_6 \subset D_{12}$, and even-order modes (i.e., those with $m = 2k$) cannot be excited either because $D_{4k} \cap D_{12} = D_l$ with $l \geq 4$; see Fig. 4(c)]. Figure 4(d) illustrates these peculiarities with an example.

As can be seen, a variety of optical responses can be obtained by using different lattice models. This is a very interesting property of the EP-WGMs supported by hole arrays, which can be exploited to develop novel polarizers and filters. For instance, in a square lattice, the quadrupolar mode is only excited for p-polarized waves, for which the transmittance is almost zero. That is, the structure transmits normally incident and off-normal s-polarized waves, while it rejects off-normal p-polarized waves, even for very small incidence angles and with a low frequency dispersion.

D. Influence of the film thickness

To gain additional insight into the physics underlying the response of the hole array, a parametric study of the film thickness and its effects on the excitation of EP-WGM is performed. Figure 5 depicts the absorption spectra of a hole array with $a = 400$ nm, $r = 160$ nm, $\theta = 2°$, and varying t. Depending on the value of t, three different regimes can be identified in Fig. 5(a). In the case of thick films ($t > 400$ nm), a single EP-WGM, highly confined to the rim of the input interface, is excited. In this case, $T = 0$ and $A \approx 0.5$. These features may allow

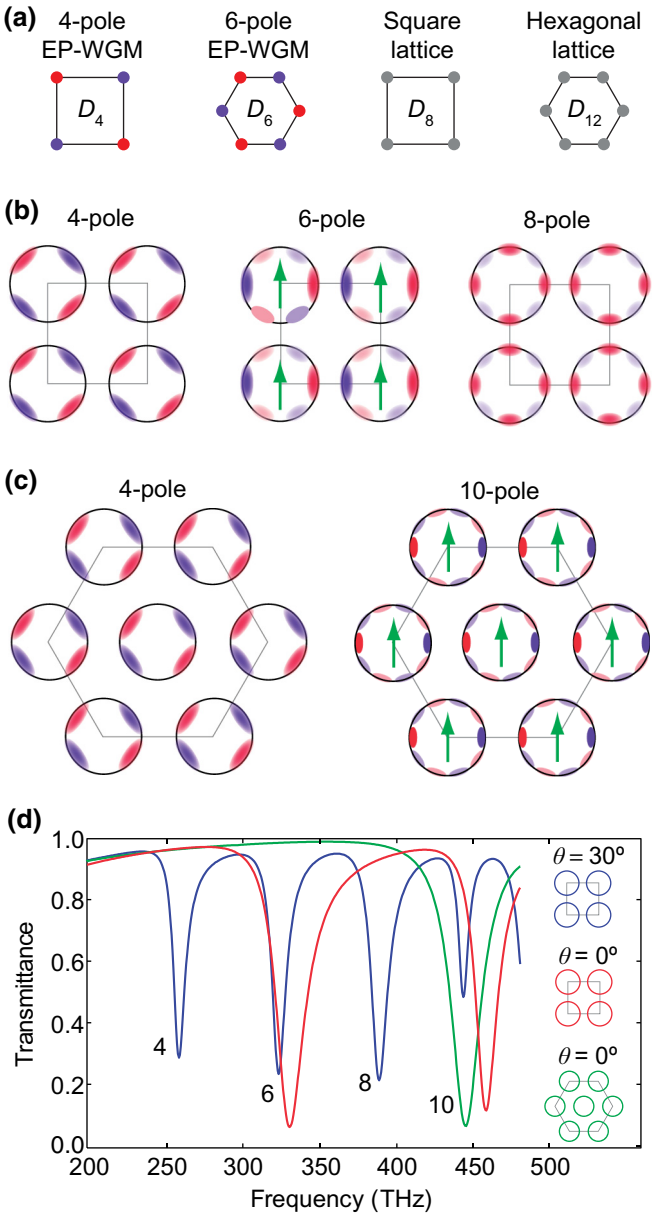

FIG. 4. The influence of the lattice symmetries on the hole-array optical response. (a) The symmetry groups of the second- and third-order EP-WGMs (4- and 6-pole) and of the square and hexagonal lattices (those of a four-sided and a six-sided polygon, respectively). (b),(c) The H_z distribution that may arise from the interactions between adjacent holes is shown for different EP-WGM orders in (b) a square lattice and (c) a hexagonal lattice. The red areas correspond to positive magnitudes while the blue areas indicate negative values. The appearance of a dipole moment is indicated with a green arrow. (d) The transmittance spectra of a hole array with $t = 5$ nm, $r = 160$ nm, and $a = 400$ nm for different lattice and/or angle configurations. The number of poles is indicated next to each resonance.

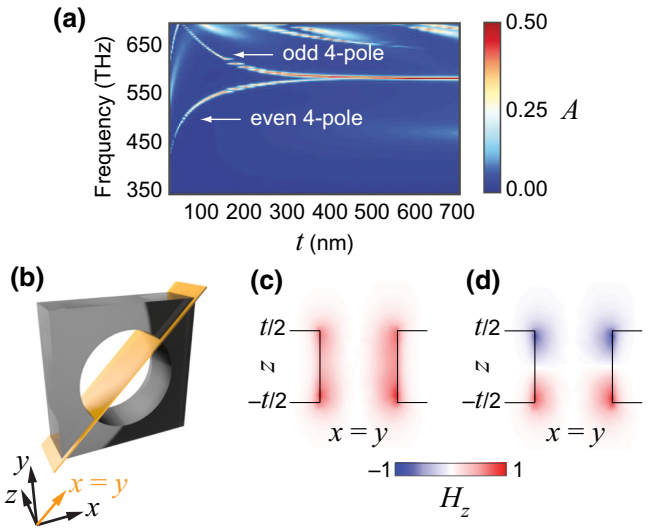

FIG. 5. The influence of the thickness and mode hybridization. (a) The absorption spectrum as a function of t for $a = 400$ nm and $r = 160$ nm. The angle of incidence is $\theta = 2°$. (b) A schematic representation of a cut plane $(x = y, z)$ passing through the center of the hole. (c),(d) The H_z distribution through the cut plane shown in (b) for $t = 300$ nm at (c) $f = 579.3$ THz and (d) $f = 592.7$ THz. The black lines indicate the location of the metal film.

the construction of low-dispersion absorbers with just one metal film (either polarization dependent or independent, by using the appropriate EP-WGM order). Note that this kind of zero-transmission absorber usually requires two metallic films (one of them patterned) separated by a dielectric [37]. For medium-thick films (50 nm $< t <$ 400 nm), the two interfaces come close enough for the input EP-WGM to evanescently excite a second one at the output interface. Hybridization results in the resonance splitting up into symmetric and antisymmetric WGMs of the same order resonating at different frequencies. This is further confirmed in Figs. 5(c) and 5(d), which show the H_z distribution at a diagonal cut plane [Fig. 5(b)] for $t = 300$ nm at the resonant frequencies of both modes. Specifically, at $f = 579.3$ THz, H_z is in phase at both hole ends (symmetric mode), while the EP-WGMs at each interface are out of phase at $f = 592.7$ THz (antisymmetric mode). Lastly, for thin films ($t < 50$ nm), the two hybridized modes become a unique mode, with a resonant frequency that rapidly decreases with t. This feature could be used to obtain low-frequency resonances with compact resonators [see the examples in Fig. 4(d)]. The case of $t \to 0$ is especially interesting. In practice, such a 2D structure may consist of a sheet of monolayer graphene perforated with antidots. Recent studies on the plasmonic properties of antidot arrays indicate a close relation with ultrathin hole arrays [38]. Moreover, in analogy to the results reported for structured thin metal films, edge plasmons have already been observed in graphene nanoribbons, disks, and slit waveguides [39–41]. Therefore, one might expect plasmonic WGMs to arise along the edges of graphene nanoholes.

E. Localized surface plasmon resonance sensors with ultrahigh figures of merit

One of the most important applications of WGMs is related to the high Q factors that they can exhibit [4]. This is an essential characteristic of the studied EP-WGMs as well. For instance, the Q factor associated with the quadrupolar resonance of the studied nanoholes is 81 (for $t = 50$ nm), with a corresponding narrow line width [defined as the full width at half maximum (FWHM) of an EP-WGM dip [42,43]) of 7.3 nm; see Fig. 6(b)]. Actually, higher plasmonic WGM Q factors are difficult to achieve [6] (the few cases in which this value is exceeded often rely on microstructures much larger than the studied nanoholes [6,44]), while line widths below 10 nm are considered as ultrasharp [45].

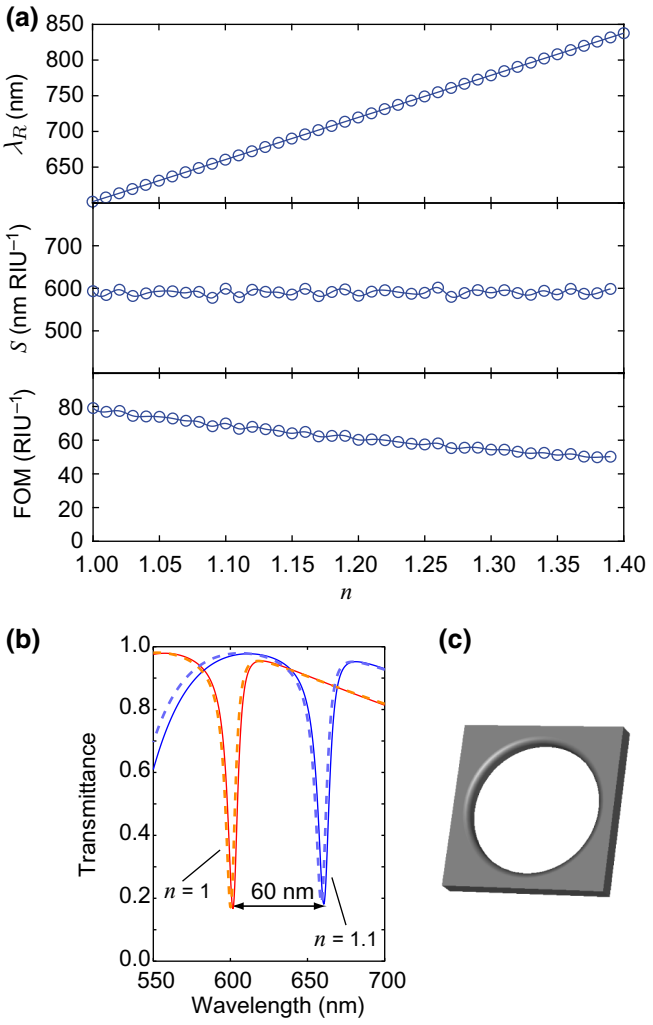

FIG. 6. The EP-WGM sensing performance in a square hole array with $t = 50$ nm, $r = 160$ nm, and $a = 400$ nm. (a) The resonant wavelength, sensitivity, and FOM as a function of n (each circle corresponds to a different simulation). (b) The variation in the transmittance as n changes from 1 to 1.1. The solid and dashed lines correspond to the simulated response of an array of holes with sharp and blended edges, respectively. (c) The unit cell with a blended-edge hole considered in the simulations.

Another relevant property of this EP-WGM is its high sensitivity to the environment [S, defined as the free-space resonant wavelength shift per background refractive index unit (RIU)], which is a sought characteristic of localized-surface-plasmon-resonance (LSPR) sensors. These devices are becoming increasingly important owing to their simplicity, low cost, and ability to probe nanoscale sensing volumes and to observe nearby molecular interactions [42,46,47]. To evaluate the potential of the quadrupolar EP-WGM as the basis of an index sensor, we simulate the transmittance of the corresponding nanohole array for a set of background index values (n) ranging from 1 to 1.4 in steps of 0.01. The free-space resonant wavelength λ_R and sensitivity for each value of n are shown in Fig. 6(a). It can be seen that λ_R varies almost linearly with n (a desirable feature of plasmonic sensors), yielding an approximately constant sensitivity $S \approx 600\ \mathrm{nm\,RIU^{-1}}$ in the considered range, which covers both gas- and liquid-sensing applications. This implies a sensitivity dynamic range of at least 0.4 RIU, typically regarded as a high value [48]. As an example, Fig. 6(b) depicts the transmittance for $n = 1$ and $n = 1.1$. Under this index change, λ_R experiences a 60-nm shift, which is consistent with the obtained sensitivity value.

The main quality parameter of plasmonic sensors is the so-called figure of merit (FOM), which is defined as the ratio of sensitivity to line width (FOM $= S/\mathrm{FWHM}$), being below 5–10 in most cases [42,47]. When combined, the reduced line width and high sensitivity of this EP-WGM result in an extremely efficient sensor with a FOM around 80 at $n = 1$ [see Fig. 6(a)]. This is among the highest values reported to date for plasmonic sensors [42,46,47] and the highest for an LSPR illuminated with free-space light (higher values have been obtained for non-edge-coupled localized and distributed modes [20,43,49,50]), with the advantage that no additional bright mode is required for its excitation. The FOM gradually decreases down to 50 at $n = 1.4$, which is still a very high value for a LSPR.

Since the field is concentrated at the edges of the hole, the EP-WGM resonance may be influenced by imperfectly sharp edge shapes in real implementations, which would be especially relevant for sensing applications. To analyze this possibility, we repeat the simulations of the studied array (for $n = 1$ and $n = 1.1$), this time with the holes having a blended edge [see Fig. 6(c)]. As seen in Fig. 6(b), the EP-WGM resonances are almost unaltered by this modification. This indicates that the EP-WGM is tolerant to variations in the edge geometry.

F. Experimental observation of a quadrupolar EP-WGM

In general, the analyzed modes can also be supported by holes with noncircular shapes. Actually, a kind of EP-WGM has been experimentally measured in a metamaterial consisting of a periodic array of square holes [14]. However, that work was focused on a different optical band displaying a negative refractive index and the presence of the EP-WGM was overlooked. Specifically, we find that the zero-transmission band appearing at approximately 1.6 eV (774 nm) in Fig. 4 of [14] corresponds to a quadrupolar EP-WGM. This can be verified by simulating the magnetic field in the hole at the mentioned wavelength, which has a quadrupolar profile and is concentrated at the hole edges [Fig. 7(a)]. To better fit the actual shape of the fabricated structures, a square hole with round angles is considered in the numerical calculation. The simulation domain is discretized by using a tetrahedral mesh optimized through an adaptive-refinement algorithm [see Fig. 7(b)].

Note that the aforementioned zero-transmission band splits into two as the incidence angle increases. The reason is that, in this case, the structure under consideration consists of a stack of two metallic hole arrays ($t = 35$ nm) separated by a 30-nm-thick dielectric layer. As a consequence, the EP-WGM of each hole array hybridizes and splits into symmetric and antisymmetric modes. This is not to be confused with the hybridization appearing in medium-thick films. The thin-film regime applies in this case and a single EP-WGM per film is excited. This analysis explains the results (band diagram) reported in Ref. [14]. In turn, such results constitute an experimental validation of the theory presented here. Moreover, this example illustrates the difference between EP-WGMs and waveguide modes. In particular, in Ref. [14], the first-order waveguide mode is identified with the transmission band appearing at 667 nm, while the second-order (quadrupolar) EP-WGM is excited at considerably longer wavelengths (consequently, the first-order resonance would appear at even larger wavelengths).

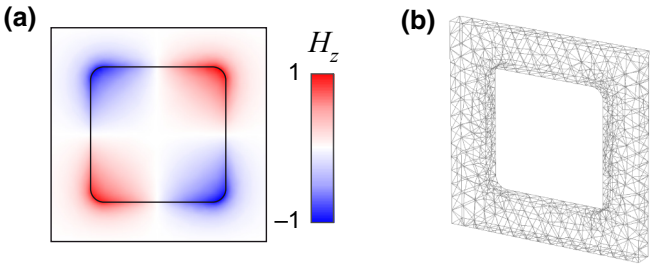

FIG. 7. A quadrupolar EP-WGM supported by a square array (periodicity $a = 400$ nm) of square holes (side $l = 250$ nm) with round corners (bending radius $b = 25$ nm) milled in a film with $t = 35$ nm. (a) The simulated H_z field. (b) The tetrahedral mesh employed in the simulation.

III. CONCLUDING REMARKS

This work shows that, in addition to the rich variety of phenomena supported by nanoholes (e.g., waveguide resonances), EP-WGMs in the form of whispering-gallery modes may also be excited and may strongly influence the spectral response of both isolated nanoholes and 2D arrays. Therefore, an understanding of EP-WGMs is crucial to better explain the optical response of nanohole-based plasmonic structures, as well as to prevent interference that may degrade their intended performance in relevant applications such as extraordinary optical transmission and metamaterials (e.g., negative index media).

The EP-WGMs studied here further exhibit some remarkable features. First, by appropriately selecting the type of lattice in 2D nanohole arrays, it is possible to select which orders are excited, while the mode behavior strongly depends on the film thickness. This in turn provides the designer with a simple and yet powerful and versatile tool to tailor the optical response of these structures. As an application example, thick films can be used to build zero-transmittance absorbers with a single metal layer.

Second, some EP-WGMs present unusually narrow line widths under specific configurations, which is useful in applications such as optical filtering and spectroscopy. In combination with the uncommon polarization dependence of the EP-WGM resonances, this property can be employed to design special polarizers.

Lastly, the ultrahigh sensing FOM that some EP-WGMs exhibit is of particular importance as an alternative and more efficient mechanism to build LSPR sensors, with application in the detection of nanoscale analytes, as well as in the observation of molecular interactions.

ACKNOWLEDGMENTS

C.G.-M. acknowledges support from the Spanish State Research Agency and the European Regional Development Fund (project TEC2015-73581-JIN PHUTURE) and from Generalitat Valenciana through the VALi+d postdoctoral program (exp. APOSTD/2014/044). G.C.B. acknowledges the funding support from the Engineering and Physical Sciences Research Council (EPSRC) (Grant No. EP/L015110/1). C.M.-S. acknowledges support from the European Seventh Framework Programme project DORADA (Grant No. IAPP-2013-610691). C.G.-M. designed the research. M.L.-C., G.C.B., and C.G.-M. performed the simulations and interpreted the data. M.L.-C. and C.G.-M. wrote the paper. M.L.-C., G.C.B., C.G.-M., and C.M.-S. critically reviewed the work. C.G.-M. and C.M.-S. played supervisory roles.

[1] C. Liu and J. A. Golovchenko, Surface Trapped X Rays: Whispering-Gallery Modes at $\lambda = 0.7$Å, Phys. Rev. Lett. **79**, 788 (1997).

[2] B. Gayral, J. M. Gérard, A. Lemaître, C. Dupuis, L. Manin, and J. L. Pelouard, High-Q wet-etched GaAs microdisks containing InAs quantum boxes, Appl. Phys. Lett. **75**, 1908 (1999).

[3] P. L. Stanwix, M. E. Tobar, P. Wolf, M. Susli, C. R. Locke, E. N. Ivanov, J. Winterflood, and F. van Kann, Test of Lorentz Invariance in Electrodynamics Using Rotating Cryogenic Sapphire Microwave Oscillators, Phys. Rev. Lett. **95**, 040404 (2005).

[4] K. J. Vahala, Optical microcavities, Nature **424**, 839 (2003).

[5] S. I. Bozhevolnyi, V. S. Volkov, E. Devaux, J-Y. Laluet, and T. W. Ebbesen, Channel plasmon subwavelength waveguide components including interferometers and ring resonators, Nature **440**, 508 (2006).

[6] B. Min, E. Ostby, V. Sorger, E. Ulin-Avila, L. Yang, X. Zhang, and K. Vahala, High-Q surface-plasmon-polariton whispering-gallery microcavity, Nature **457**, 455 (2009).

[7] P. Berini, Plasmon-polariton waves guided by thin lossy metal films of finite width: Bound modes of symmetric structures, Phys. Rev. B **61**, 10484 (2000).

[8] F-P. Schmidt, H. Ditlbacher, U. Hohenester, A. Hohenau, F. Hofer, and J. R. Krenn, Universal dispersion of surface plasmons in flat nanostructures, Nat. Commun. **5**, 3604 (2014).

[9] J. Prikulis, P. Hanarp, L. Olofsson, D. Sutherland, and M. Käll, Optical spectroscopy of nanometric holes in thin gold films, Nano Lett. **4**, 1003 (2004).

[10] T. Rindzevicius, Y. Alaverdyan, B. Sepulveda, T. Pakizeh, M. Käll, R. Hillenbrand, J. Aizpurua, and F. J. García de Abajo, Nanohole plasmons in optically thin gold films, J. Phys. Chem. C **111**, 1207 (2007).

[11] A. Degiron, H. Lezec, N. Yamamoto, and T. Ebbesen, Optical transmission properties of a single subwavelength aperture in a real metal, Opt. Commun. **239**, 61 (2004).

[12] T. Coenen and A. Polman, Optical properties of single plasmonic holes probed with local electron beam excitation, ACS Nano **8**, 7350 (2014).

[13] L. Rayleigh, CXII. The problem of the whispering gallery, Philos. Mag. Ser. **6 20**, 1001- (1910).

[14] C. García-Meca, J. Hurtado, J. Martí, A. Martínez, W. Dickson, and A. V. Zayats, Low-Loss Multilayered Metamaterial Exhibiting a Negative Index of Refraction at Visible Wavelengths, Phys. Rev. Lett. **106**, 067402 (2011).

[15] P. B. Catrysse and S. Fan, Propagating plasmonic mode in nanoscale apertures and its implications for extraordinary transmission, J. Nanophotonics **2**, 021790 (2008).

[16] M. Liu, Y. Song, Y. Zhang, X. Wang, and C. Jin, Mode evolution and transmission suppression in a perforated ultrathin metallic film with a triangular array of holes, Plasmonics **7**, 397 (2012).

[17] M. Nishida, N. Hatakenaka, and Y. Kadoya, Multipole surface plasmons in metallic nanohole arrays, Phys. Rev. B **91**, 235406 (2015).

[18] Lumerical Solutions, Inc., FDTD tool of LUMERICAL DEVICE Multiphysics Simulation Suite, http://www.lumerical.com/tcad-products/fdtd/.

[19] P. B. Johnson and R. W. Christy, Optical constants of the noble metals, Phys. Rev. B **6**, 4370 (1972).

[20] A. A. Yanika, A. E. Cetina, M. Huanga, A. Artara, S. H. Mousavic, A. Khanikaevc, J. H. Connord, G. Shvets, and H. Altug, Seeing protein monolayers with naked eye through plasmonic Fano resonances, Proc. Natl. Acad. Sci. USA **108**, 11784 (2011).

[21] F. J. García-Vidal, L. Martín-Moreno, E. Moreno, L. K. S Kumar, and R. Gordon, Transmission of light through a single rectangular hole in a real metal, Phys. Rev. B **74**, 153411 (2006).

[22] R. Gordon, L. S. Kumar, and A. Brolo, Resonant light transmission through a nanohole in a metal film, IEEE Trans. Nanotech. **5**, 291 (2006).

[23] Z. Ruan and M. Qiu, Enhanced Transmission through Periodic Arrays of Subwavelength Holes: The Role of Localized Waveguide Resonances, Phys. Rev. Lett. **96**, 233901 (2006).

[24] S. Yokogawa, S. P. Burgos, and H. A. Atwater, Plasmonic color filters for CMOS image sensor applications, Nano Lett. **12**, 4349 (2012).

[25] K. Konishi, T. Higuchi, J. Li, J. Larsson, S. Ishii, and M. Kuwata-Gonokami, Polarization-Controlled Circular Second-Harmonic Generation from Metal Hole Arrays with Threefold Rotational Symmetry, Phys. Rev. Lett. **112**, 135502 (2014).

[26] S. Jeon, J-H. Lee, J-H. Jeong, Y. S. Song, C-K. Moon, J-J. Kim, and J. R. Youn, Vacuum nanohole array embedded phosphorescent organic light emitting diodes, Sci. Rep. **5**, 8685 (2015).

[27] D. R. Smith, J. B. Pendry, and C. K. Wiltshire, Metamaterials and negative refractive index, Science **305**, 788 (2004).

[28] T. W. Ebbesen, H. J. Lezec, H. F. Ghaemi, T. Thio, and P. A. Wolff, Extraordinary optical transmission through subwavelength hole arrays, Nature **391**, 667 (1998).

[29] C. Genet and T. Ebbesen, Light in tiny holes, Nature **445**, 39 (2007).

[30] J. Bravo-Abad, A. Degiron, F. Przybilla, C. Genet, F. J. García-Vidal, L. Martín-Moreno, and T. W. Ebbesen, How light emerges from an illuminated array of subwavelength holes, Nat. Phys. **2**, 120 (2006).

[31] H. Liu and P. Lalanne, Microscopic theory of the extraordinary optical transmission, Nature **452**, 728-731 (2008).

[32] A. Y. Nikitin, F. J. García-Vidal, and L. Martín-Moreno, Surface Electromagnetic Field Radiated by a Subwavelength Hole in a Metal Film, Phys. Rev. Lett. **105**, 073902 (2010).

[33] J. Parsons, E. Hendry, C. P. Burrows, B. Auguié, J. R Sambles, and W. L. Barnes, Localized surface-plasmon resonances in periodic nondiffracting metallic nanoparticle and nanohole arrays, Phys. Rev. B **79**, 073412 (2009).

[34] R. W. Wood, XLII. On a remarkable case of uneven distribution of light in a diffraction grating spectrum, Phylos. Mag. **4**, 396 (1902).

[35] R. W. Wood, Anomalous diffraction gratings, Phys. Rev. **48**, 928 (1935).

[36] M. Meier, P. F. Liao, and A. Wokaun, Enhanced fields on rough surfaces: Dipolar interactions among particles of

sizes exceeding the Rayleigh limit, J. Opt. Soc. Am. B **2**, 931 (1985).
[37] C. M. Watts, X. Liu, and W. J. Padilla, Metamaterial electromagnetic wave absorbers, Adv. Mater. **24**, OP98 (2012).
[38] A. Y. Nikitin, F. Guinea, and L. Martín-Moreno, Resonant plasmonic effects in periodic graphene antidot arrays, Appl. Phys. Lett. **101**, 151119 (2012).
[39] Z. Fei, M. D. Goldflam, J.-S. Wu, S. Dai, M. Wagner, A. S. McLeod, M. K. Liu, K. W. Post, S. Zhu, G. C. A. M. Janssen, M. M. Fogler, and D. N. Basov, Edge and surface plasmons in graphene nanoribbons, Nano Lett. **15**, 8271 (2015).
[40] A. Y. Nikitin, P. Alonso-González, S. Vélez, S. Mastel, A. Centeno, A. Pesquera, A. Zurutuza, F. Casanova, L. E. Hueso, F. H. L. Koppens, and R. Hillenbrand, Real-space mapping of tailored sheet and edge plasmons in graphene nanoresonators, Nat. Photon. **10**, 239 (2016).
[41] P. A. D. Gonçalves, S. Xiao, N. M. R. Peres, and N. A. Mortensen, Hybridized plasmons in 2D nanoslits: From graphene to anisotropic 2D materials, ACS Photonics **4**, 3045 (2017).
[42] L. Tong, H. Wei, S. Zhang, and H. Xu, Recent advances in plasmonic sensors, Sensors **14**, 7959 (2014).
[43] B. Liu, S. Chen, J. Zhang, X. Yao, J. Zhong, H. Lin, T. Huang, Z. Yang, J. Zhu, S. Liu, C. Lienau, L. Wang, and B. Ren, A plasmonic sensor array with ultrahigh figures of merit and resonance linewidths down to 3 nm, Adv. Mater. **30**, 1706031 (2018).
[44] X. Zhang, Z. Ma, H. Yu, X. Guo, Y. Ma, and L. Tong, Plasmonic resonance of whispering gallery modes in an Au cylinder, Opt. Express **19**, 3902 (2012).
[45] S. H. Lee, T. W. Johnson, N. C. Lindquist, H. Im, D. J. Norris, and S-H. Oh, Linewidth-optimized extraordinary optical transmission in water with template-stripped metallic nanohole arrays, Adv. Funct. Mater. **22**, 4439 (2012).
[46] J. Anker, W. Hall, O. Lyandres, N. Shah, J. Zhao, and R. van Duyne, Biosensing with plasmonic nanosensors, Nat. Mater. **7**, 442 (2008).
[47] K. Mayer and J. Hafner, Localized surface plasmon resonance sensors, Chem. Rev. **111**, 3828 (2011).
[48] Y.-C. Cheng, Y.-J. Chang, Y.-C. Chuang, B.-Z. Huang, and C.-C. Chen, A plasmonic refractive index sensor with an ultrabroad dynamic sensing range, Sci. Rep. **9**, 5134 (2019).
[49] R. Zafar and M. Salim, Enhanced figure of merit in Fano resonance-based plasmonic refractive index sensor, IEEE Sens. J., **15**, 6313 (2015).
[50] L. Chen, Y. Liu, Z. Yu, D. Wu, R. Ma, Y. Zhang, and H. Ye, Numerical analysis of a near-infrared plasmonic refractive index sensor with high figure of merit based on a fillet cavity, Opt. Express **24**, 9975 (2016).